PNAS RESEARCH ARTICLE | APPLIED PHYSICAL SCIENCES
DEVELOPMENTAL BIOLOGY

Static morphogen scaling enables proportional growth in a tissue growth model inspired by axolotl limb regeneration

Natalia Lyubaykina[a], Dunja Knapp[b,c,1], Pietro Tardivo[d,e], Maximilian Kotz[a], Tatiana Sandoval-Guzmán[b,c,f,1], and Benjamin M. Friedrich[a,1]

Affiliations are included on p. 8.

Edited by Charles Peskin, New York University, New York, NY; received February 10, 2025; accepted October 4, 2025

Axolotls can regenerate lost limbs throughout life, while they continue to grow. This poses the question of how the size and pattern of a regenerating limb is matched to a widely varying animal size. Two interacting signaling molecules, Sonic Hedgehog (SHH) and Fibroblast Growth Factor (FGF8), are produced at opposite sides of the regenerating limb and sustain tissue growth through a pair of oppositely oriented signaling gradients. As the size of the regrowing tissue can vary more than three-fold depending on the size of the animal, it is unclear how the activities of these mutually dependent morphogens are maintained and subsequently terminated to determine appropriate growth. Scaling of limb regeneration suggests a size-dependent adaptation of morphogen gradient parameters. Inspired by this biological example, we theoretically investigate general mechanisms of morphogen-controlled growth arrest and proportional growth. In the proposed mechanism, tissue growth increases the spatial distance between the two morphogen gradients, which eventually arrests morphogen activity and growth. We put forward two distinct scaling scenarios of morphogen gradients: either dynamic scaling with blastema size, where morphogen gradient parameters change dynamically with the growing tissue, or static scaling with animal size, where morphogen gradient parameters stay constant during blastema growth and only depend on animal size. We show that static scaling ensures proportional growth, but dynamic scaling does not. We compare theory predictions to experimental quantification of SHH and FGF8 morphogen gradient parameters at different time-points of regeneration in different-sized animals, indicating static scaling for some morphogen parameters, which is sufficient to ensure proportional growth in our model.

regeneration | axolotl | adaptive morphogenesis | growth control | morphogen gradient scaling

Significance

Regeneration of lost body parts must not just recapitulate developmental programs, but also adjust to the size of the adult organism. The control mechanisms enabling such size-adaptive morphogenesis are not well understood. Here, we propose a simple, yet effective mechanism for robust growth arrest by a pair of oppositely oriented morphogen gradients, which together promote growth. Tissue growth decreases the overlap between both gradients and eventually halts morphogen signaling and arrests tissue growth. Our study advances concepts underlying regeneration, applicable to salamanders that can regrow limbs that match the widely varying size of adults. It also highlights the connection between development and regeneration, outlining general conditions for proportional growth, with potential implications for limb development in nonregenerative species.

Axolotls possess remarkable regenerative capabilities, including the ability to regenerate fully functional limbs even in adulthood (1). Limb regeneration shares similarities with limb development (2, 3), which is largely conserved among vertebrates (4). However, limb regeneration must also cope with the different sizes of juvenile and adult animals (Fig. 1*A*), which can differ up to ten-fold in linear size (5). Regeneration to match animal size represents a general open problem of adaptive morphogenesis (6). Limb regeneration in axolotls starts with wound closure after limb loss, followed by the formation of a bud called blastema consisting of undifferentiated progenitor cells, growth of this blastema, and eventually cell differentiation to give rise to various limb tissues (Fig. 1*B*). Blastema growth depends on animal size (Fig. 1*C*; wide-field images of corresponding stages; see *SI Appendix*, Fig. S1). The result of the first phase of blastema growth is a hypometric limb (called "tiny limb" in ref. 7). This hypometric limb subsequently grows to its final size in a second growth phase, which is particularly pronounced in larger animals (7).

We will focus on the first growth phase of limb regeneration, blastema growth. The sizes of same-stage blastemas scale with animal size (8). This scaling is not perfectly proportional, but allometric, i.e., blastema size does not increase linearly with animal size, but according to a power-law with exponent 0.6 (8) (see also *SI Appendix*, Fig. S2). In contrast, intact limb size is proportional to animal size across a wide range of animal sizes (8) (*SI Appendix*, Fig. S3). Thus, the relative size of the blastema is smaller in larger animals. For the smaller animals considered here, proportional scaling is an appropriate approximation.

Blastema growth involves a pair of oppositely oriented morphogen gradients. Like the developing limb bud, the regenerating blastema displays two signaling centers that secrete morphogens: a posterior center expressing SHH (Sonic Hedgehog) (9, 10), and an anterior center expressing FGF8 (Fibroblast Growth Factor) (11, 12), which mutually

The authors declare no competing interest.

This article is a PNAS Direct Submission.

[1]To whom correspondence may be addressed. Email: dunja.knapp@tu-dresden.de, tatiana.sandoval_guzman@tu-dresden.de, or benjamin.m.friedrich@tu-dresden.de.

This article contains supporting information online at https://www.pnas.org/lookup/suppl/doi:10.1073/pnas.2503086122/-/DCSupplemental.

Published November 20, 2025.

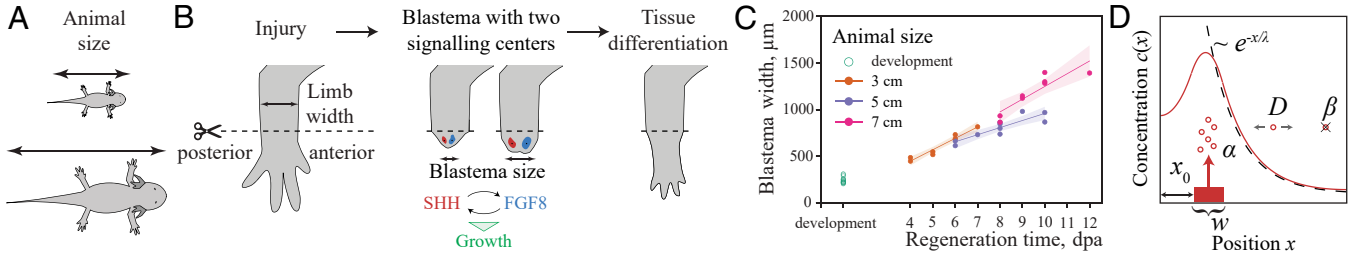

Fig. 1. Axolotl limb regeneration. (*A*) Schematic of axolotls of different sizes. (*B*) Schematic of axolotl limb regeneration, highlighting its key stages: After limb amputation, a blastema with two distinct signaling centers producing SHH posteriorly (red) and FGF8 anteriorly (blue) forms. These mutually reinforcing morphogens induce cell proliferation, and thus regulate blastema growth. After this first growth phase of blastema growth, tissue differentiation and additional growth completes limb regeneration. The dashed line indicates the amputation plane; arrows indicate limb and blastema size. (*C*) Blastema size at subsequent time points (days post amputation, dpa) for animals of different size (filled symbols), and development (open symbols; measured along a line passing through the centers of SHH and FGF source regions in 3D images; see *Materials and Methods* for details). (*D*) Morphogen gradient described by minimal reaction–diffusion model Eq. **1** together with visualization of model parameters.

reinforce each other's expression (13–15). In intact mature limbs, SHH and FGF8 are undetectable (16, 17) (see also *SI Appendix*, Fig. S4). However, following injury, their production is activated, with clear evidence that both SHH and FGF8 are essential for maintaining blastema growth and successful limb regeneration (9, 11, 17). Because of their mutual feedback, the individual roles of SHH and FGF8 in regulating cell proliferation are challenging to disentangle. While neither morphogen alone seems sufficient to support growth and regeneration in ectopically induced blastemas in vivo (17), both enhance proliferation individually and additively in cultured dissociated blastema cells in vitro (8). Consequently, it remains challenging to determine whether one or both morphogens directly up-regulate proliferation.

Here, we focus on the stage of blastema growth as a paradigmatic model system for morphogen-dependent growth control and growth arrest in animals of different sizes. Recently, the sizes of the source regions of SHH and FGF8 were measured by chromogenic RNA in situ stainings in thin sections of middle-stage blastemas of animals of different sizes, indicating allometric scaling of source regions with animal size at the chosen time-point (8). Inspired by this, we explore a minimal mathematical model of coupled tissue growth and morphogen dynamics in a system of two morphogens to identify physical mechanisms that ensure robust growth arrest and proportional growth. We systematically dissect differences between two fundamental growth rules based on either one or two morphogens, as well as two scaling scenarios of morphogen gradients, scaling either dynamically with growing blastema size, or statically with animal size. Our theoretical analysis singles out a mechanism of growth control by two oppositely oriented morphogen gradients, where at least some morphogen gradient parameters must exhibit static scaling to enable proportional growth. By combining whole mount in situ hybridization with tissue clearing and confocal microscopy (18), we quantify the three-dimensional size of SHH and FGF8 morphogen sources as a function of time in regenerating blastemas of different-sized animals, as well as the FGF8 signaling range by measuring the expression of its downstream target *Dusp6*. We found that some gradient parameters (FGF8 source size) scale statically with animal size, while others scale dynamically with blastema size. Such scaling is sufficient to ensure proportional growth in our model.

Results

Coupling Morphogen Dynamics and Growth. As a minimal model of morphogen dynamics in a growing blastema, we consider a one-dimensional system of size L, see Fig. 1*D*. We first introduce notation for the simple case of a single morphogen. The morphogen is produced within a source region of width w (located at a distance x_0 from the tissue boundary), subsequently diffuses through the tissue with effective diffusion coefficient D, while undergoing degradation with degradation rate β. The dynamics of morphogen concentration $c(x,t)$ as a function of time t is then given by

$$\partial_t c(x,t) = D\,\partial_x^2 c(x,t) - \beta c(x,t) + \alpha\,\chi_w(x). \qquad [1]$$

Here, the source function $\chi_w(x)$ characterizes the shape of the morphogen source, which we assume to take the value 1 inside the interval $[x_0, x_0+w]$ and zero outside. The rate total of morphogen production is thus $j = \alpha w$, with units of molecules per time. The steady-state morphogen concentration profile $c^*(x)$ that is established at long times is thus fully defined by five parameters, which set its amplitude A and a characteristic pattern length-scale λ. This pattern length-scale is determined by a competition between the diffusion coefficient D and the degradation rate β

$$\lambda = \sqrt{\frac{D}{\beta}}. \qquad [2]$$

The steady-state concentration gradient $c^*(x)$ approximately follows an exponentially decaying profile with this pattern length-scale λ

$$c^*(x) \approx \frac{\alpha w}{\sqrt{D\beta}} \exp\left(-\frac{x}{\lambda}\right). \qquad [3]$$

This approximation becomes exact when the morphogen source is small, localized on the system's boundary, and the system is large. Analytic formulas for more realistic cases are given in *SI Appendix*, Eq. **S18**. Generally, concentrations are higher in smaller, bounded systems, as morphogens spread in a smaller domain. This size dependence of morphogen concentrations will become important in our model, once morphogens control growth.

Eq. **1** generalizes in a straightforward manner to the case of two morphogens with respective concentration fields $s(x,t)$ and $f(x,t)$ instead of $c(x,t)$ in Eq. **1**, where $s(x)$ and $f(x)$ can be thought of as the concentrations of SHH and FGF8 morphogens. For conceptual clarity, we consider a symmetric case of two morphogens with identical kinetic parameters and mirror-symmetric source regions (see *SI Appendix*, Eqs. **S24** and **S25** for their formulas analogous to Eq. **1**). The general case of nonidentical parameters for two morphogens is qualitatively similar.

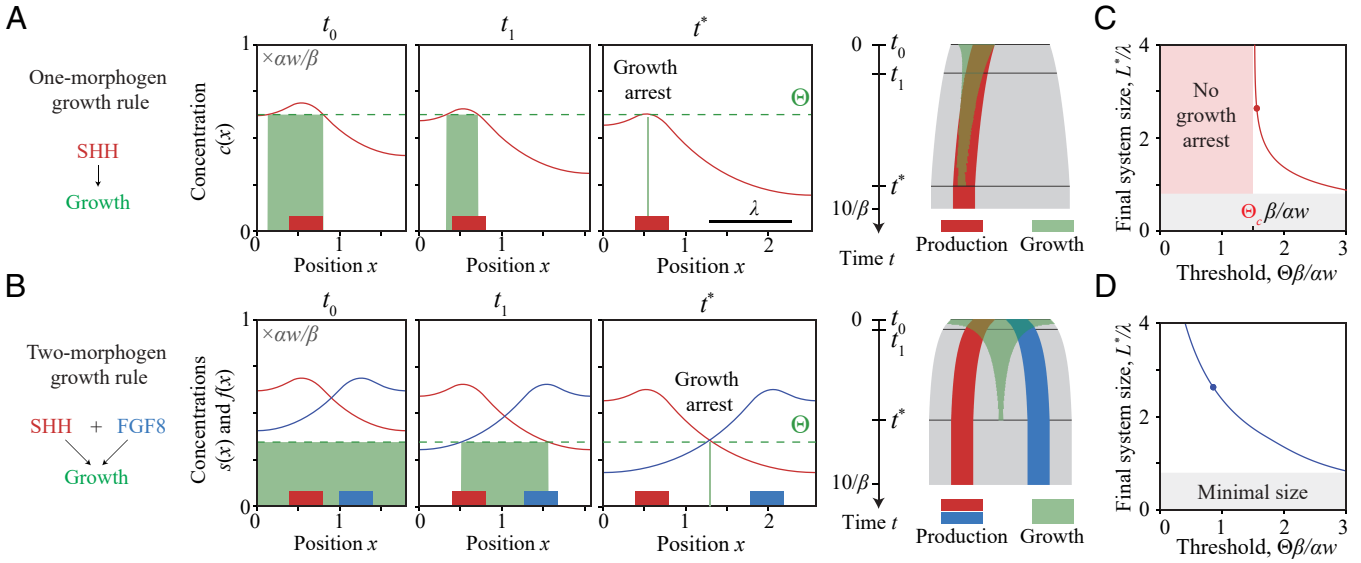

Fig. 2. Two putative growth rules. (*A*) Schematic of one-morphogen growth rule: The tissue grows where the concentration $c(x)$ of a single morphogen is above the growth threshold Θ. Morphogen source region (red region), morphogen gradient (red curve), growth threshold Θ (dashed green line), and growth zone (green region) at different time points. A corresponding kymograph of simulated tissue growth until growth arrest is shown to the *Right* (gray: tissue, red: morphogen source, green: growth zone with $c(x) > \Theta$). (*B*) Schematic of two-morphogen growth rule: A tissue grows only where the concentrations of both morphogens are above the growth threshold Θ. Morphogen gradients (red, blue) of the two morphogens at different time points, analogous to panel (*A*). A kymograph shows production regions of both morphogens (red, blue). (*C*) Final system size L^* normalized by pattern length-scale λ as a function of a normalized growth threshold $\Theta\beta/\alpha w$ for the one-morphogen growth rule. Θ_c indicates the critical threshold below which the one-morphogen growth rule fails to arrest growth. (*D*) Final system size L^* normalized by pattern length-scale λ as a function of normalized growth threshold $\Theta\beta/\alpha w$ for the two-morphogen growth rule. Threshold parameter and final system size in panels (*A* and *B*) are indicated by a point in panels (*C* and *D*), respectively. Parameters: *SI Appendix*, Table S1; lengths are plotted relative to characteristic length $\lambda = 1$; concentrations are plotted relative to characteristic concentration $\alpha w/\beta = 0.4$.

To address the dynamics in growing tissue, we consider a one-dimensional tissue that grows with local growth rate $g(x, t)$. Tissue growth convects the concentration field $c(x, t)$ of morphogen with velocity $v(x, t)$, where $\partial_x v = g$, as well as dilutes local morphogen concentration at rate g (*Materials and Methods*).

Growth Control by One or Two Morphogens. Two interacting morphogens, SHH and FGF8, are implicated in regulating cell proliferation in axolotl limb development and regeneration (8, 17). Due to the mutual feedback between these two morphogens, inactivating one consequently inactivates the other. Therefore, it is experimentally difficult to determine if the direct signal from just one or from both morphogens is needed to promote proliferation. To theoretically explore both cases, we define two putative growth rules, both of which are inspired by a switch-like control of cell behavior as a function of local morphogen concentration (19). Specifically, we assume that the tissue grows locally if morphogen concentrations are above a threshold:

One-morphogen growth rule: the tissue grows at the position x if (and only if) the concentration $c(x)$ of a morphogen is above a fixed threshold Θ; see Fig. 2*A*.

Two-morphogen growth rule: the tissue grows at the position x if the concentrations of both morphogens, $s(x)$ and $f(x)$ (e.g., SHH and FGF8) are above a fixed threshold Θ; see Fig. 2*B*.

For the sake of simplicity, we assume a symmetric scenario with equal threshold Θ for both $s(x)$ and $f(x)$ for the two-morphogen growth rule. A more general case can be mapped to this special case by a simple rescaling. Source width (w) and position (x_0) are kept constant; more realistic scenarios of source growth are explored in the next section.

We numerically simulated morphogen dynamics according to Eq. **1** in a system with reflecting boundary conditions of dynamic size $L(t)$, coupled with growth of this system assuming either the one- and two-morphogen growth rule; see Fig. 2. For both growth rules, the amplitudes of the morphogen gradients decrease as the system grows. Consequently, for the one-morphogen growth rule, the growth zone where morphogen levels exceed the threshold ($c(x, t) > \Theta$) shrinks at its border opposite to the source, until—for suitable parameter choices—growth eventually arrests (Fig. 2*A*). For the two-morphogen growth rule, the growth zone where the levels of both morphogens exceed the threshold ($s(x, t) > \Theta$ and $f(x, t) > \Theta$) shrinks even faster and at both borders, as the two opposing morphogen profiles overlap less when the system grows (Fig. 2*B*).

Fig. 2 *C* and *D* show the final system size L^* at growth arrest for the one- and two-morphogen growth rule, respectively. For the one-morphogen growth rule, growth arrests only if the growth threshold Θ exceeds a critical value Θ_c, where $\Theta_c = \alpha w/(D\beta)^{1/2}$ for the limit case of a point source region (for details, see *SI Appendix*, Eq. **S28**); for $\Theta < \Theta_c$, the system will grow indefinitely (Fig. 2*C*). For the two-morphogen growth rule, growth always arrests for any threshold (Fig. 2*D*). Since we consider a source with constant size and position, and the source region should fit into the system, the size of the system should be at least $w + x_0$, setting a minimal size. While we considered an idealized case where growth is slower than the dynamics of the morphogens, implying that morphogen gradients are always in quasi-steady state, numerical simulations reveal qualitatively similar behavior when this assumption is relaxed (*SI Appendix*, Fig. S5). In *SI Appendix*, we also give analytic formulas for the final system size L^* as a function of the growth threshold Θ for the limit case of a point source region (*SI Appendix*, Eqs. **S27** and **S30**). There, we also analyzed the sensitivity of the final system size L^* to the model parameters (*SI Appendix*, Fig. S6), and found that the two-morphogen growth rule is less sensitive to parameter variations and ensures growth arrest for a wider range of parameters. Further, the two-morphogen growth rule arrests

growth even for open or absorbing boundary conditions, while the one-morphogen growth rule requires reflecting boundary conditions (*SI Appendix*, Fig. S10). This basic model shows that morphogen-dependent tissue growth can self-terminate, but does not include any scaling. Next, we investigate how tissues can attain the correct, proportionate final size through growth arrest in animals of different sizes.

Dynamic vs. Static Scaling of Morphogen Gradients. In the generic model of growth control from the preceding section, the final system size L^* only depends on the initially defined morphogen gradient parameters. In axolotl limb regeneration, the final limb size depends on animal size, suggesting that some parameters of morphogen gradients should be size-dependent. In an idealized scenario of proportional growth, the final size L^* of the system should be proportional to animal size L_a. Similarly, blastema size at the beginning of regeneration increases with animal size (Fig. 1*C*). Hence, in a simplified scenario, we assume that the initial system size L_0 is proportional to animal size L_a. To investigate how scaling of morphogen parameters could affect tissue growth, we investigate different scenarios for the size dependence of morphogen parameters.

We say that a morphogen gradient scales with a size ℓ if at least one of its features, source width w or pattern length-scale λ, both of which affect the signaling range, scales with this size ℓ. We distinguish two fundamentally different scaling scenarios, which differ by different interpretations of ℓ:

- dynamic scaling with growing blastema size $L(t)$, corresponding to the choice $\ell = L(t)$, and
- static scaling with animal size L_a, i.e. $\ell = L_a$.

For each of these two main scenarios, we consider three subscenarios. In all three subscenarios, we assume that the source region width and its position scale as $w \sim \ell$ and $x_0 \sim \ell$. In the first subscenario, which we term source scaling, the pattern length-scale λ is independent of size ℓ, see Fig. 3, *Left* columns. In two additional subscenarios, in addition to source width, also the pattern length-scale scales as $\lambda \sim \ell$. According to Eq. **2**, either the effective diffusion coefficient D or the morphogen degradation rate β must change with ℓ. This defines a second and third subscenario, which we refer to as D-scaling (i.e., $D \sim \ell^2$), and β-scaling ($\beta \sim \ell^{-2}$), respectively, see Fig. 3, *Middle* and *Right* columns. The three subscenarios affect gradient amplitude A in

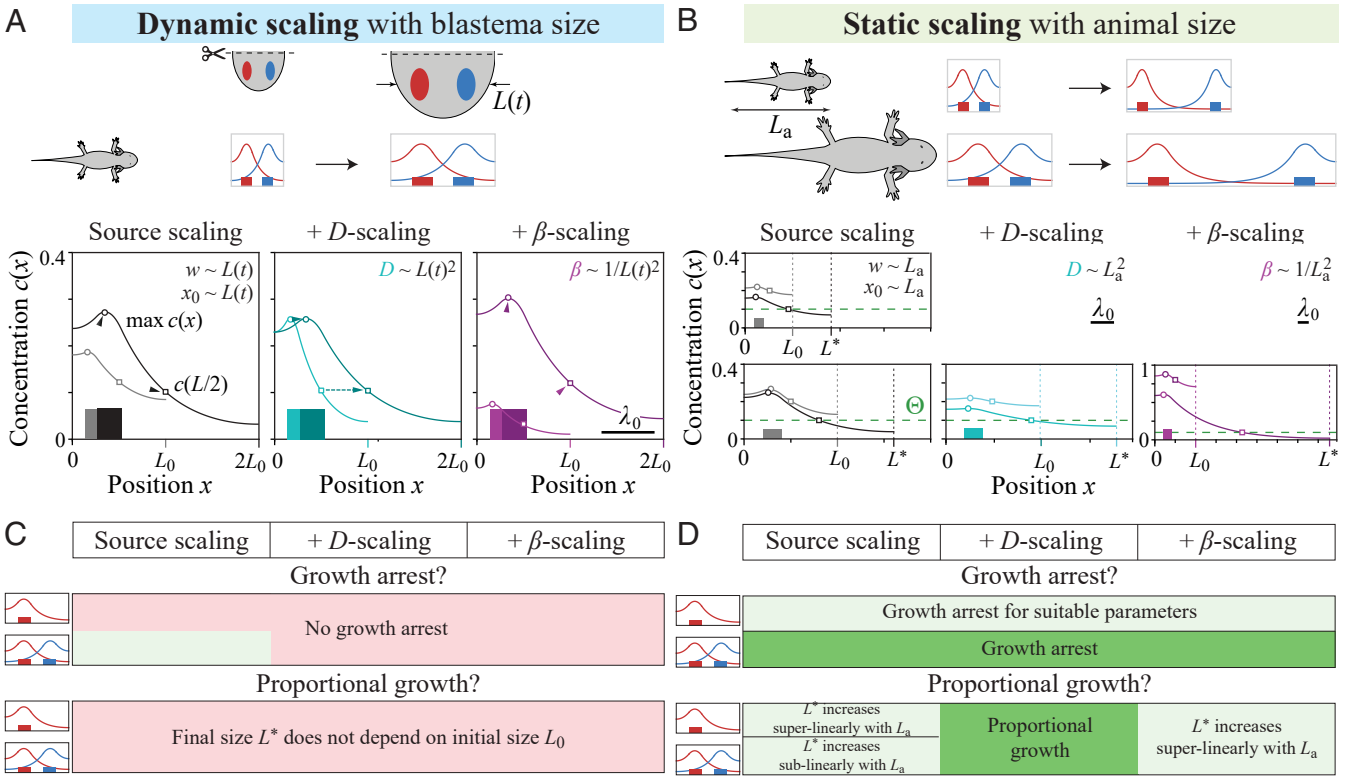

Fig. 3. Two scenarios of morphogen gradient scaling. (*A*) Schematic of dynamic scaling: morphogen gradients scale with growing blastema size $L(t)$. Different subscenarios of dynamic scaling affect the amplitude of morphogen gradients differently (source scaling with production rate $\alpha \sim L(t)$: black, *D*-scaling with effective diffusion coefficient $D \sim L(t)^2$: cyan, β-scaling with degradation rate $\beta \sim 1/L(t)^2$: magenta); see text for details. For each subscenario, source regions (boxes) and morphogen profiles (solid lines) are shown for initial tissue size L_0 and when tissue size has doubled in lighter and darker color, respectively. For simplicity, the second morphogen is not shown; its profile is mirror-symmetric for the chosen symmetric parameters. For the one-morphogen growth rule, the system grows if the amplitude (circle) exceeds a threshold Θ; for the two-morphogen growth rule with symmetric morphogen profiles, the system grows if the concentration at the midpoint of the system (square) exceeds Θ. (*B*) Schematic of static scaling with animal size: parameters of morphogen dynamics depend on animal size, but remain constant during growth. Same subscenarios of scaling as in panel (*A*), but parameters of morphogen dynamics now depend on animal size L_a. Shown are morphogen gradients at the beginning of growth with initial system size L_0 (assumed proportional to L_a for simplicity) and at growth arrest with final system size L^* for two values of L_0 (*Upper* and *Lower* row). (*C*) Summary of modeling predictions for dynamic scaling with blastema size, corresponding to the three scaling subscenarios introduced in panel (*A*). For dynamic scaling, growth arrests for any growth threshold Θ for the two-morphogen growth rule if the morphogen source scales yet not the pattern length-scale λ, but not for any other subscenario. However, even in the scenario with growth arrest, the final system size L^* is independent of initial system size, i.e. there is no proportional growth. (*D*) Summary of modeling predictions for static scaling with animal size, corresponding to the three scaling subscenarios introduced in panel (*B*). For static scaling, morphogen dynamics parameters remain constant during growth. Correspondingly, growth arrests for any growth threshold Θ for the two-morphogen growth rule (introduced in Fig. 2), yet for the one-morphogen rule only if the growth threshold Θ exceeds a critical value Θ_c. Proportional growth is achieved for the *D*-scaling subscenario, where both the effective diffusion coefficient *D* and the source region scales with animal size. Parameters: *SI Appendix*, Table S1.

different ways (*SI Appendix*, Table S2): A increases with increasing size ℓ for source scaling, and even more so for β-scaling, where in addition to scaling of the source also the degradation rate β decreases for larger ℓ. In the case of D-scaling, the amplitude A stays approximately constant, as the effects of the source scaling and of the increase in diffusion cancel each other. Dynamic scaling has been reported in several systems (20–27), and shall therefore be analyzed first.

Dynamic scaling with blastema size. In the absence of scaling, both the one-morphogen and the two-morphogen growth rules enable growth arrest. If the morphogen gradients exhibit dynamic scaling, model parameters and thus morphogen concentrations change dynamically with the growing blastema size $L(t)$. For most scenarios of dynamic scaling, concentrations stay approximately constant or even increase, and hence growth does not arrest anymore, see Fig. 3*A*. The only exception is growth arrest for the special case when the pattern length-scale λ does not scale, and the two-morphogen rule is assumed. We obtain similar results without scaling of the source (*SI Appendix*, Table S2). More generally, if either size w or position x_0 of the morphogen source scale, we obtain a combinatorial set of 32 subscenarios: growth arrests in 13 of these subscenarios for the two-morphogen growth rule, but only 4 subscenarios for the one-morphogen growth rule (*SI Appendix*, Figs. S7–S9). However, even if growth arrests, the final system size L^* is independent of the initial system size L_0. Thus, in the case of dynamic scaling with growing blastema size, proportional growth is not possible.

Scaling with animal size. Next, we explore the scenario of scaling with animal size, where the parameters of the morphogen dynamics are set by the animal size L_a and then remain constant during blastema growth. This could occur if those parameters are set by systemic factors (e.g. hormonal or metabolic). As parameters of the morphogen dynamics remain constant during blastema growth, for animals of fixed size, the system behaves exactly the same way as in the case without scaling. We conclude that growth will arrest under minimal assumptions as described in Fig. 2. However, the final blastema size L^* now depends on the animal size L_a in a nontrivial manner; see Fig. 3*D*. Proportional growth with $L^* \sim L_a$ is obtained exactly for D-scaling. For β-scaling, L^* increases superlinearly with L_a. These predictions are robust, and we obtain similar results, e.g., in the limit case of a point source (*SI Appendix*, Table S2). While Fig. 3 focused on the limit case of slow growth $g \ll \beta$, we observe virtually the same proportional growth for the two-morphogen growth rule (and variants thereof with graded growth response) if growth is fast (*SI Appendix*, Fig. S5). Similarly, results virtually do not change if instead of the reflecting boundary conditions used in Fig. 3, we assume either open or absorbing boundary conditions, with the exception of the one-morphogen growth rule, which does not facilitate growth arrest for these alternative boundary conditions (*SI Appendix*, Fig. S10). This, once more, highlights the robustness of the two-morphogen growth rule.

Combination of dynamic and static scaling. While Fig. 3*C* shows that dynamic scaling alone cannot ensure proportional growth, intriguingly, a combination of dynamic and static scaling can. For example, a scenario where all SHH parameters exhibit dynamic scaling and all FGF parameters exhibit static scaling ensures proportional growth over a five-fold range of initial system sizes if D-scaling (i.e., size-dependent regulation of effective diffusion coefficients) is assumed (*SI Appendix*, Fig. S11). This remains true even if all morphogen parameters—except FGF source size—exhibit dynamic scaling. In fact, the structure of the mathematical model implies that if growth arrest occurs for any form of D-scaling, combining dynamic and static scaling of different morphogen parameters, growth must be proportional with $L^* \sim L_a$ (*SI Appendix*).

Quantification of Size-Dependent Morphogen Gradients. To assess putative scaling of morphogen gradients in regenerating axolotl limb blastema, we quantitatively analyzed SHH and FGF8 source regions in 3D in animals of different sizes and at several different regeneration time points. We used Hybridization Chain Reaction (HCR) RNA in situ, combined with tissue clearing and confocal microscopy to perform 3D quantitative measurements of SHH and FGF8 gradient parameters in developing limb buds and in regenerating limb blastemas from animals of three different sizes (snout-to-tail animal size: 3 cm, 5 cm, 7 cm). Measurements were taken at multiple time points (days post amputation, dpa) throughout the period when both signaling centers were present; see Fig. 4*A*. We first quantified blastema size along the line in 3D passing through SHH and FGF8 source region centers as in Fig. 1*C*; see Fig. 4*B*. Next, we quantified the linear sizes of SHH and FGF8 source regions by computing the cubic root of the volume enclosed by the 50%-isosurfaces of the respective mRNA signals, which defines a length-scale that characterizes source size. We also quantified the gap size x_0 between the source regions and the tissue boundary corresponding to the source position. Finally, the spatial range of FGF8 signaling was inferred from the volume enclosed by the 50%-isosurface of *Dusp6* mRNA, a well-established downstream target of FGF8 signaling (28–30). All morphogen gradient parameters exhibit a clear size dependence. Yet, distinguishing dynamic and static scaling is complicated by the fact that blastema size and animal size are correlated (*SI Appendix*, Figs. S2 and S3). We first tested both a linear regression as a function of blastema size (*Left* column in Fig. 4*D*), and a linear regression as a function of animal size (*Right* column). For both fit scenarios, we obtained satisfactory fits, with statistically significant size dependence, suggesting that both static and dynamic scaling may contribute to the observed size-dependent patterns. A contribution of dynamic scaling is suggested by the temporal increase of gradient parameters within some animal size groups, see *SI Appendix*, Fig. S12. On the other hand, static scaling with animal size is compatible with the data, with R^2 values only slightly smaller or even larger than those of the linear regression against blastema size. To gain further insight, we performed a partial correlation analysis on these data, which allows testing for conditional statistical independence (*SI Appendix*, Table S3): After factoring out the influence of animal size, less than 0.1% of the remaining variance of FGF8 source width w could be explained by blastema size, with no statistically significant correlation. In contrast, an analogous analysis for SHH source size revealed a much higher explained variance of 58% with high significance levels $P < 0.1\%$, indicative of a contribution of dynamic scaling for SHH. The statistical analysis for the other morphogen parameters suggests different contributions of static and dynamic scaling, see Fig. 4*D* and *SI Appendix*. In conclusion, the data for the FGF8 source region and possibly other morphogen gradient parameters are compatible with static scaling. Note that in our model, it is sufficient if only a subset of morphogen parameters, e.g. only FGF8 source size, exhibit static but not dynamic scaling, to ensure growth arrest and proportional growth (*SI Appendix*, Fig. S11).

Mutual Feedback Between Morphogens. Previous works suggested a mutual feedback between SHH and FGF production (13–15). Above, we assumed that both morphogens are produced independently of each other and their source regions and production rates remain constant during tissue growth without

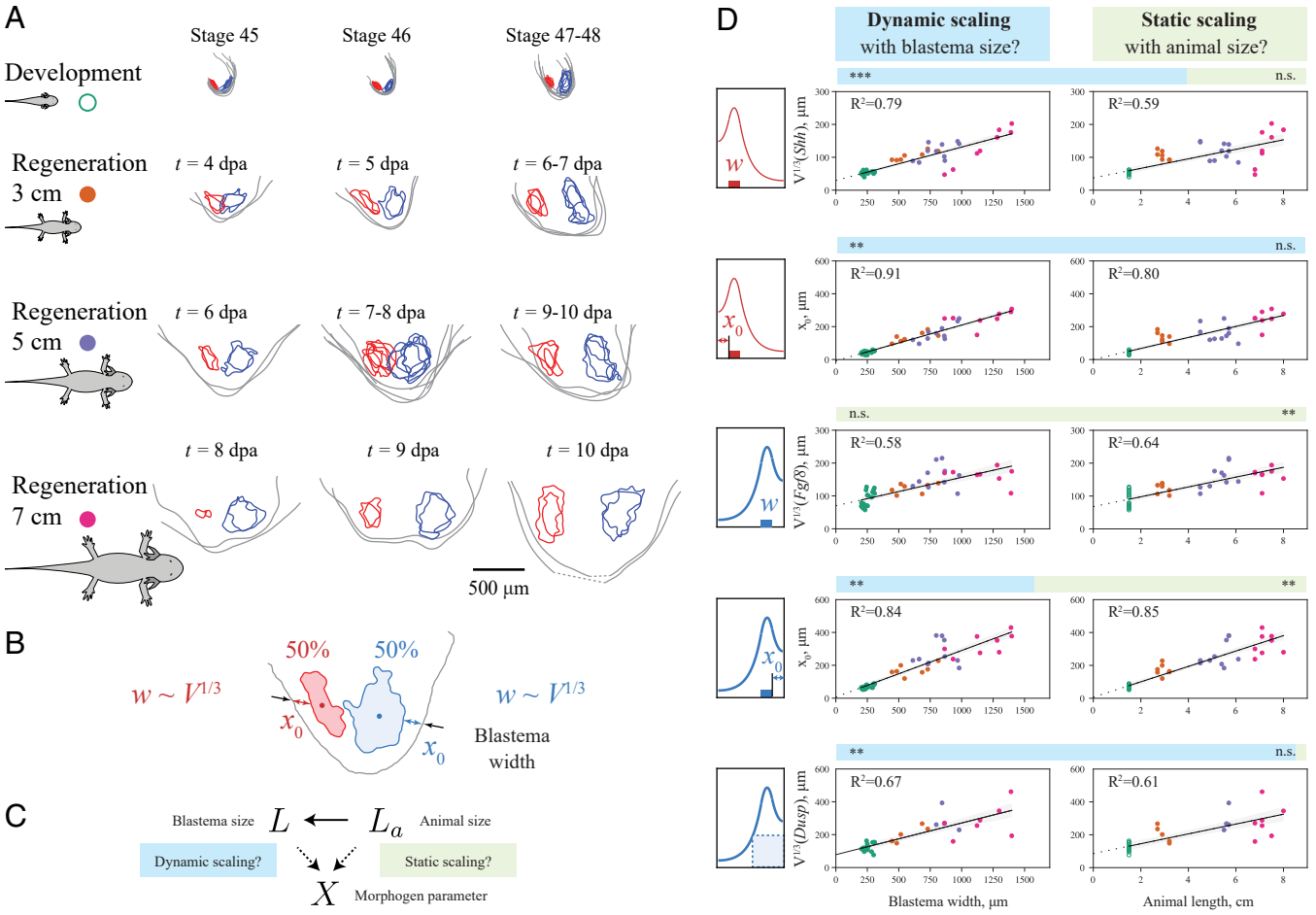

Fig. 4. Size dependence of SHH and FGF8 morphogen gradients. (*A*) Outlines of SHH and FGF8 source regions from in situ hybridization in limb buds at different developmental stages, as well as regenerating blastemas of different-sized animals and at different regeneration time points (*Shh*: red, *Fgf8*: blue, 50% threshold of normalized intensity, shown as binary projections along dorsal–ventral axis on plane containing the centers of the *Shh* and *Fgf8* regions; see *SI Appendix* for details; by convention, italicized names, e.g. *Shh* and *Fgf8*, refer to mRNA, indicating morphogen production, while capitalized names, e.g. SHH and FGF8, refer to the corresponding proteins. (*B*) Definition of morphogen parameters: the linear source size $V^{1/3}$ determined from 3D-volume V enclosed by 50%-isosurface for *Shh* defines the source width w for SHH, the gap size between SHH source boundary and tissue boundary defines the source position x_0 [measured in 2D-projections along a line connecting the centers of the *Shh* and *Fgf8* regions as shown in panel (*A*)]; analogous definitions for *Fgf8*. We determined a proxy for the FGF8 signaling range as $V^{1/3}$ from the 3D-volume V enclosed by the 50%-isosurface of the FGF8 target *Dusp6*. (*C*) A morphogen parameter X may exhibit either dynamic scaling with blastema size L, or static scaling with animal size L_a. Since L and L_a are correlated, causal inference is needed to test these scenarios. (*D*) Morphogen parameters as defined in panel (*B*) as a function of blastema width (*Left* column) and animal length (*Right* column). Colors represent animal size as in panel (*A*) and Fig. 1*C* (filled circles: regeneration, open green circles: development; linear regression: black). For each morphogen parameter, a bar plot represents the result of a partial correlation analysis (statistical significance and proportion of residual variance from a test for the respective opposite null hypothesis, indicative of dynamic scaling (blue, null hypothesis: only static scaling), and static scaling (green, null hypothesis: only dynamic scaling); see *SI Appendix* for details).

specifying biological mechanisms of maintaining morphogen production. Here, we theoretically describe a possible minimal feedback scenario. We assume that there are regions competent for SHH or FGF8 production (shown as transparent regions in Fig. 5*A*). This assumption is supported by distinct properties of anterior and posterior blastema regions (16, 31–33). We further assume that SHH and FGF8 are produced in their respective competent region if the opposite morphogen concentration is above a feedback threshold Θ_{fb}. With such mutual feedback, the system can be in one of two limiting regimes, depending on the relative magnitude of the growth threshold Θ and the feedback threshold Θ_{fb}. In the first regime, growth arrests because the growth threshold is reached first (green region in Fig. 5*B*). The system thus behaves similar to the case without feedback described above and arrests growth, while morphogen production is still ON. In the second regime, the feedback threshold is reached first (orange region in Fig. 5*B*). As a consequence, the source regions of morphogen production shrink rapidly, and morphogen production is switched OFF. Without morphogen production, also tissue growth arrests. In this second regime, the feedback between the two morphogens functions as a tissue-level ON/OFF switch for growth. While Fig. 5*B* shows results for the two-morphogen growth rule, the system behaves qualitatively similarly for the one-morphogen growth rule. Signaling delays of morphogen feedback would result in a gradual decrease of morphogen profile amplitudes, but otherwise similar behavior.

Adding feedback to the system thus does not significantly change its behavior with regard to growth arrest, demonstrating that our conclusions remain applicable also in a more realistic model. Feedback between the two morphogens could be a means of avoiding the slow fade-out of growth observed without feedback (Fig. 2), or even of switching off growth homogeneously throughout the system.

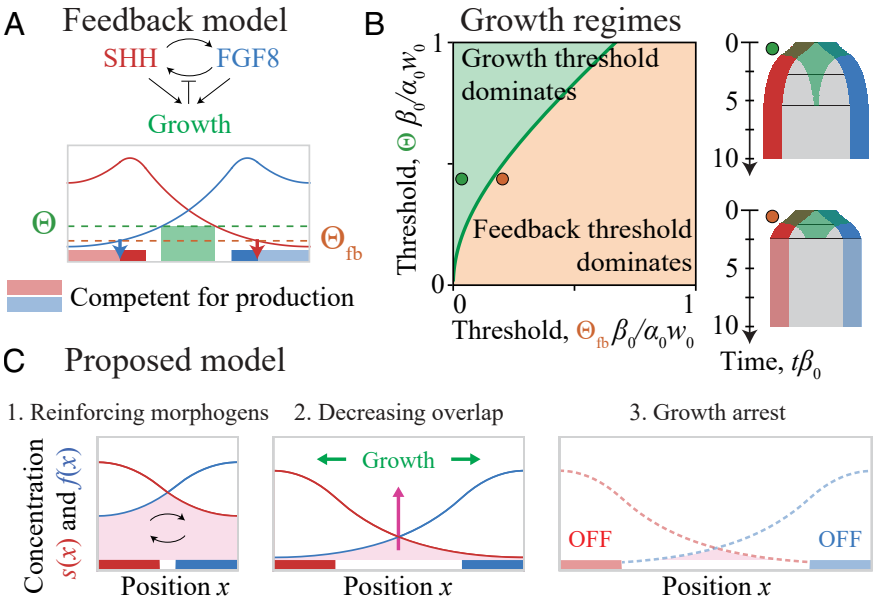

Fig. 5. Feedback model of reinforcing morphogens. (*A*) Minimal model of mutual feedback between oppositely oriented morphogen gradients: Each morphogen can only be produced in a region of competent cells (transparent red and blue bars) where the concentration of the respective other morphogen exceeds a threshold (Θ_{fb}, orange dashed), defining two source regions (solid red and blue bars). (*B*) Phase diagram of growth regimes as a function of growth threshold Θ and feedback threshold Θ_{fb}, here shown for the two-morphogen growth rule, exhibiting two regimes: The growth threshold Θ dominates, resulting in dynamics analogous to the case without feedback (green) as in Fig. 2, or, the feedback threshold Θ_{fb} dominates, resulting in instantaneous and homogeneous growth arrest across the entire system (orange). (*C*) Model of growth arrest by the growth-threshold regime: 1. The tissue grows (green) where both morphogens (red and blue) are above the growth threshold (green dashed). 2. Tissue growth pushes the two morphogen sources apart, thus decreasing the region where the two morphogens overlap. 3. Due to the mutual feedback between the two morphogens, their respective source regions start shrinking rapidly, switching off both morphogens and arresting growth.

Discussion

Inspired by the size-adaptive regeneration of axolotl limbs, we addressed the general question of how morphogen-dependent tissue growth can be arrested once a tissue has reached its correct size. In our prototypical minimal model, tissue growth is induced by a threshold rule for either a single morphogen, or a pair of oppositely oriented morphogen gradients. The two-morphogen growth rule with two oppositely oriented gradients provides a particularly robust mechanism of growth arrest: The overlap between the two gradients induces growth; this growth increases the spatial separation between the two morphogen sources and thus decreases the overlap between the two gradients. This negative feedback loop robustly terminates growth at a specific tissue size. Proportional growth, however, where the final system size is proportional to initial size, requires scaling of morphogen gradients. We distinguished two fundamental scaling scenarios: dynamic scaling of morphogen gradients with the growing blastema, or static scaling, where morphogen gradient parameters depend on animal size, but remain constant during growth. Our theoretical analysis shows that static scaling with animal size of at least a subset of morphogen parameters is necessary and sufficient for proportional growth if a switch-like growth rule is assumed (Fig. 3 and *SI Appendix*, Fig. S11). We obtain similar results for graded growth responses (*SI Appendix*, Fig. S5). Thus, different growth and feedback rules consistently yield robust growth arrest and proportional growth in the model. Yet, the spatiotemporal patterns of local tissue growth can differ (*SI Appendix*, Fig. S13), which could help discriminating model variants in future experiments.

Blastema growth in axolotl regeneration is more complex. Our analysis addresses only the first stage of blastema outgrowth, which is followed by cell differentiation and a second growth phase. The second phase, which is independent of SHH–FGF signaling, is thought to be regulated by neuronal signals (7). Nevertheless, the first growth phase and the blastema size at the onset of tissue differentiation is important to ensure accurate limb patterning, including the correct number of bone elements.

Our model assumed reflecting boundary conditions along the anterior–posterior axis of SHH–FGF signaling. Indeed, the epidermis surrounding the blastema is expected to act as a diffusion barrier for spreading morphogens. However, morphogens may diffuse along the proximo–distal axis from the blastema into the limb stump at early stages, with ECM components possibly limiting morphogen outflux from the blastema, resulting in more complex boundary conditions. Reflecting boundary conditions near the source are important for the one-morphogen growth rule, while the two-morphogen growth rule works for different boundary conditions (*SI Appendix*, Fig. S10).

Interestingly, blastema growth is not proportional to limb size in very large animals ($\gtrsim$10 cm), and is more accurately described by allometric scaling laws (8) (confirmed also in *SI Appendix*, Fig. S2). This suggests limits of scaling. Note that subscenarios of our model can reproduce allometric scaling laws as observed experimentally (*SI Appendix*, Fig. S9). While our minimal model showed that exclusively dynamic scaling cannot enable proportional growth, it is likely that a combination of dynamic and static scaling applies in axolotl. Furthermore, dynamic scaling could still be compatible with proportional blastema growth if a separate timer mechanism terminates growth after a fixed time.

We used in situ hybridization in 3D tissues to quantify SHH and FGF8 source regions and FGF8 signaling range in developing limb buds and regenerating blastemas of different sizes at different time points. We find a clear size dependence of morphogen gradient parameters. In particular, our data suggest static scaling with animal size for the FGF8 source region size, while the SHH source region size may exhibit dynamic scaling. This extends the recently published in situ hybridization analysis

of source sizes in tissue slices for a single morphological stage in ref. 8. Our analysis of growth control by scaling morphogen gradients is independent of the particular implementation of morphogen scaling, and only depends on which parameters of morphogen dynamics are adjusted in a size-dependent manner. Scaling of morphogen gradients has been reported in a number of systems (20–27). A common concept in proposed mechanisms is the presence of a modulator such as an "expander," whose concentration regulates, e.g., the effective diffusion coefficient or degradation rate of a morphogen (34–37). In expander-dilution models, tissue growth dilutes the concentration of the expander inversely proportional to tissue volume (38). In expander-repression models, the production of the expander depends on the morphogen itself (34). Recently, SCUBE family molecules were shown to affect SHH spreading (39) and suggested to act by an expansion-repression mechanism to control the amplitude and pattern length-scale of the SHH gradient in the zebrafish neural tube (40), compatible with a mechanism of *D*-scaling.

SHH and FGF8 also guide limb development in other vertebrates (2, 3). This pair of morphogen gradients must be switched on, but later also switched off again. Previous mathematical models focused on the temporal dynamics of morphogens (15), including the role of intermediate morphogens Bone Morphogenetic Protein (BMP) and Gremlin (GREM), which itself are thought to be a part of the SHH–FGF feedback loop. To explain how SHH and FGF become switched off again, various hypotheses reviewed in ref. 41 were put forward: A first hypothesis suggests that the medial portion of the SHH competent region, which previously expressed SHH, loses this competence, creating an expanding region of cells that are not competent to express either SHH or GREM or FGF8 (42). A second hypothesis suggests that FGF8 terminates GREM in a concentration-dependent manner (43); alternatively, a low concentration of BMP could activate GREM at early stages, while a higher concentration of BMP could suppress GREM later (44). We comment that these hypotheses would require signal delays to prevent becoming trapped in an intermediate state between "on" and "off." Another hypothesis would be a timer mechanism that switches off SHH and FGF after a preset growth period (45). These hypotheses not only underline the intricate molecular interactions involved in the growth control of developing and regenerating limbs but also start to appreciate the importance of spatial patterns of signaling.

Our model proposes that a coupling of spatial patterns and growth provides a simple and robust mechanism by which the SHH–FGF feedback loop could become switched off after the first stage of blastema outgrowth is completed (Fig. 5*C*). Our minimal model suggests specific experiments. Quantifying SHH and FGF8 morphogen gradients as a function of animal size and time, ideally by measuring protein concentrations instead of down-stream signaling, will allow testing our theory prediction of static scaling with animal size (or limb size). Cell culture experiments with controlled levels of morphogens as initiated in ref. 8 could test the growth rules proposed here. This could pave the road toward more realistic, data-driven models that capitalize on the concepts laid out in the idealized, one-dimensional model studied here. In conclusion, we proposed a simple mechanism of two oppositely oriented morphogen gradients that reinforce each other, to enable robust growth arrest and proportional tissue growth by scaling of morphogen parameters with animal size.

Materials and Methods

Numerical Methods. In the presence of tissue growth with local growth rate $g(x, t)$, Eq. **1** changes to

$$\partial_t c(x,t) = D\,\partial_x^2 c - v(x,t)\partial_x c - [\beta + g(x,t)]c + \alpha\,\chi_{w(t)}(x), \quad \textbf{[4]}$$

where $\partial_x v = g$ (21, 46). This equation is numerically solved using a modified Euler scheme in a Lagrangian frame with nonuniform spatial grid, whose bin sizes Δx_i are updated according to $\Delta x_i(t_{n+1}) = [1 + g(x_i, t_n)\Delta t]\,\Delta x_i(t_n)$.

Whole-Mount HCR In Situ Hybridization and Imaging. *Shh*, *Fgf8*, and *Dusp6* mRNAs were detected in formaldehyde-fixed limb blastema and developing limb buds obtained from different-sized animals at different timepoints by whole mount HCR, a fluorescent RNA in situ method as described in ref. 47 with minor modifications, followed by refractive index matching and confocal imaging in 3D (for detailed protocol, see *SI Appendix*).

Image Analysis. For analysis of 3D multichannel z-stack images, blastemas were segmented using APOC (48) trained with user-specified ground truth labels applied to the *Shh* channel using Napari (49) and custom Python code. Blood vessels detected in the autofluorescence channel were segmented using APOC, and the corresponding binary mask was excluded from all channels. The linear size of SHH and FGF8 source regions, as well as of FGF8 signaling indicated by *Dusp6* mRNA, were determined as the cubic roots of the volumes enclosed by the respective 50%-isointensity surfaces (after denoising and min-max normalization of each channel). Blastema size was measured in 3D images along a line passing through the centers of the *Shh* and *Fgf8* regions. Gap sizes between the blastema boundary and the boundaries of these source regions (x_0) were measured along the same line, yet using 2D-projections to account for a possible nonconvex shape of source regions.

Data, Materials, and Software Availability. Raw image data and Python code for growth simulations and image analysis can be accessed at a public github repository in ref. 50. All other data are included in the manuscript and/or supporting information.

ACKNOWLEDGMENTS. We thank Leo Otsuki and Elly M. Tanaka (Institute of Molecular Biotechnology of the Austrian Academy of Science) for the transgenic axolotl line (tgScel(ZRS:TFPnls-T2A-ERT2-Cre-ERT2)^{Etnka}. We thank Elly M. Tanaka, as well as all members of the Sandoval-Guzmán and Friedrich groups for stimulating discussions, the animal carers of the Center for Regenerative Therapies Dresden (Beate Gruhl and Anja Wagner) for dedicated axolotl care, the light microscopy facility of the Center for Molecular and Cellular Bioengineering for excellent support, as well as Veikko F. Geyer for statistical analysis support. T.S.-G. and B.M.F. acknowledge funding from a joint D-A-CH grant from the German and Austrian Science Foundations (441649267, jointly with Elly M. Tanaka). B.M.F. was additionally supported by the Deutsche Forschungsgemeinschaft (DFG, German Research Foundation) under Germany's Excellence Strategy–EXC-2068-390729961, as well as through a Heisenberg grant (421143374).

Author affiliations: [a]Cluster of Excellence 'Physics of Life', Dresden University of Technology, Dresden 01307, Germany; [b]Department of Internal Medicine III, University Hospital Carl Gustav Carus, Dresden University of Technology, Dresden 01307, Germany; [c]Paul Langerhans Institute Dresden, Helmholtz Centre Munich at Dresden University of Technology, Dresden 01307, Germany; [d]Institute of Molecular Biotechnology of the Austrian Academy of Sciences, Vienna BioCenter, Vienna 1030 Austria; [e]Vienna BioCenter PhD Program, Doctoral School of the University of Vienna and Medical University of Vienna, Vienna 1030, Austria; and [f]Center for Regenerative Therapies Dresden, Dresden University of Technology, Dresden 01307, Germany

Author contributions: N.L., D.K., P.T., T.S.-G., and B.M.F. designed research; N.L., D.K., M.K., and B.M.F. performed research; N.L. contributed new reagents/analytic tools; N.L., D.K., and M.K. analyzed data; and N.L., D.K., P.T., M.K., T.S.-G., and B.M.F. wrote the paper.

1. A. Simon, E. Tanaka, Limb regeneration. *Wiley Interdiscip. Rev. Dev. Biol.* **2**, 291–300 (2013).
2. K. Muneoka, S. V. Bryant, Evidence that patterning mechanisms in developing and regenerating limbs are the same. *Nature* **298**, 369–371 (1982).
3. D. Payzin-Dogru, J. L. Whited, An integrative framework for salamander and mouse limb regeneration. *Int. J. Dev. Biol.* **62**, 393–402 (2018).
4. J. J. Young, C. J. Tabin, Saunders's framework for understanding limb development as a platform for investigating limb evolution. *Dev. Biol.* **429**, 401–408 (2017).
5. W. A. Vieira, K. M. Wells, C. D. McCusker, Advancements to the axolotl model for regeneration and aging. *Gerontology* **66**, 212–222 (2020).
6. N. D. Leigh, J. D. Currie, Rebuilding limbs, one cell at a time. *Dev. Dyn.* **251**, 1389 (2022).
7. K. M. Wells, K. Kelley, M. Baumel, W. A. Vieira, C. D. McCusker, Neural control of growth and size in the axolotl limb regenerate. *eLife* **10**, e68584 (2021).
8. S. Furukawa, S. Yamamoto, A. Ohashi, Y. Morishita, A. Satoh, Allometry in limb regeneration and scale-invariant patterning as the basis of normal morphogenesis from different sizes of blastemas. *Development* **151**, dev202697 (2024).
9. M. A. Torok, D. M. Gardiner, J. C. Izpisúa-Belmonte, S. V. Bryant, Sonic hedgehog (SHH) expression in developing and regenerating axolotl limbs. *J. Exp. Zool.* **284**, 197–206 (1999).
10. C. Tickle, M. Towers, Sonic hedgehog signaling in limb development. *Front. Cell Dev. Biol.* **5**, 14 (2017).
11. M. J. Han, J. Y. An, W. S. Kim, Expression patterns of FGF-8 during development and limb regeneration of the axolotl. *Dev. Dyn.* **220**, 40–48 (2001).
12. S. Purushothaman, A. Elewa, A. W. Seifert, FGF-signaling is compartmentalized within the mesenchyme and controls proliferation during salamander limb development. *eLife* **8**, e48507 (2019).
13. E. Laufer, C. E. Nelson, R. L. Johnson, B. A. Morgan, C. Tabin, Sonic hedgehog and FGF-4 act through a signaling cascade and feedback loop to integrate growth and patterning of the developing limb bud. *Cell* **79**, 993–1003 (1994).
14. L. Niswander, S. Jeffrey, G. R. Martin, C. Tickle, A positive feedback loop coordinates growth and patterning in the vertebrate limb. *Nature* **371**, 609–612 (1994).
15. J. D. Bénazet *et al*., A self-regulatory system of interlinked signaling feedback loops controls mouse limb patterning. *Science* **323**, 1050–1053 (2009).
16. L. Otsuki, S. Plattner, Y. Taniguchi-Sugiura, F. Falcon, E. Tanaka, Molecular basis of positional memory in limb regeneration. *Nature* **642**, 730–738 (2025).
17. E. Nacu, E. Gromberg, C. R. Oliveira, D. Drechsel, E. M. Tanaka, FGF8 and SHH substitute for anterior-posterior tissue interactions to induce limb regeneration. *Nature* **533**, 407–410 (2016).
18. G. L. Glotzer, P. Tardivo, E. M. Tanaka, Canonical Wnt signaling and the regulation of divergent mesenchymal FGF8 expression in axolotl limb development and regeneration. *eLife* **11**, e79762 . (2022).
19. L. Wolpert, Positional information and the spatial pattern of cellular differentiation. *J. Theor. Biol.* **25**, 1–47 (1969).
20. D. Ben-Zvi, G. Pyrowolakis, N. Barkai, B. Z. Shilo, Expansion-repression mechanism for scaling the DPP activation gradient in *Drosophila* wing imaginal discs. *Curr. Biol.* **21**, 1391–1396 (2011).
21. O. Wartlick *et al*., Dynamics of DPP signaling and proliferation control. *Science* **331**, 1154–1159 (2011).
22. T. Stückemann *et al*., Antagonistic self-organizing patterning systems control maintenance and regeneration of the anteroposterior axis in planarians. *Dev. Cell* **40**, 248–263 (2017).
23. R. Mateus *et al*., BMP signaling gradient scaling in the zebrafish pectoral fin. *Cell Rep.* **30** , 4292–4302 (2020).
24. M. Romanova-Michaelides *et al*., Morphogen gradient scaling by recycling of intracellular DPP. *Nature* **602**, 287–293 (2022).
25. A. Kicheva, J. Briscoe, Control of tissue development by morphogens. *Annu. Rev. Cell Dev. Biol.* **39**, 91–121 (2023).
26. M. Nikolić *et al*., Scale invariance in early embryonic development. *Proc. Natl. Acad. Sci. U.S.A.* **121**, e2403265121 (2024).
27. A. Rich *et al*., Decaying and expanding ERK gradients process memory of skeletal size during zebrafish fin regeneration. bioRxiv [Preprint] (2025). https://doi.org/10.1101/2025.01.23.634576 (Accessed 1 June 2025).
28. G. A. Molina, S. C. Watkins, M. Tsang, Generation of FGF reporter transgenic zebrafish and their utility in chemical screens. *BMC Dev. Biol.* **7**, 1–14 (2007).
29. C. Li, D. A. Scott, E. Hatch, X. Tian, S. L. Mansour, Dusp6 (Mkp3) is a negative feedback regulator of FGF-stimulated ERK signaling during mouse development. *Development* **134**, 167–176 (2007).
30. M. Ekerot *et al*., Negative-feedback regulation of FGF signalling by DUSP6/MKP-3 is driven by ERK1/2 and mediated by Ets factor binding to a conserved site within the DUSP6/MKP-3 gene promoter. *Biochem. J.* **412**, 287–298 (2008).
31. B. M. Carlson, The effects of rotation and positional change of stump tissues upon morphogenesis of the regenerating axolotl limb. *Dev. Biol.* **47**, 269–291 (1975).
32. T. Endo, S. V. Bryant, D. M. Gardiner, A stepwise model system for limb regeneration. *Dev. Biol.* **270**, 135–145 (2004).
33. S. V. Bryant, Regenerative failure of double half limbs in *Notophthalmus viridescens*. *Nature* **263**, 676–679 (1976).
34. D. Ben-Zvi, N. Barkai, Scaling of morphogen gradients by an expansion-repression integral feedback control. *Proc. Natl. Acad. Sci. U.S.A.* **107**, 6924–6929 (2010).
35. S. Werner *et al*., Scaling and regeneration of self-organized patterns. *Phys. Rev. Lett.* **114**, 138101 (2015).
36. D. M. Umulis, H. G. Othmer, Mechanisms of scaling in pattern formation. *Development* **140**, 4830–4843 (2013).
37. B. Z. Shilo, N. Barkai, Buffering global variability of morphogen gradients. *Dev. Cell* **40**, 429–438 (2017).
38. O. Wartlick, P. Mumcu, F. Jülicher, M. Gonzalez-Gaitan, Understanding morphogenetic growth control - lessons from flies. *Nat. Rev. Mol. Cell Biol.* **12**, 594–604 (2011).
39. G. Schlissel, M. Meziane, D. Narducci, A. S. Hansen, P. Li, Diffusion barriers imposed by tissue topology shape hedgehog morphogen gradients. *Proc. Natl. Acad. Sci. U.S.A.* **121**, e2400677121 (2024).
40. Z. M. Collins, K. Ishimatsu, T. Y. Tsai, S. G. Megason, A Scube2-SHH feedback loop links morphogen release to morphogen signaling to enable scale invariant patterning of the ventral neural tube. bioRxiv [Preprint] (2023). https://doi.org/10.1101/469239 (Accessed 1 February 2025).
41. A. Zuniga, R. Zeller, Dynamic and self-regulatory interactions among gene regulatory networks control vertebrate limb bud morphogenesis. *Curr. Top. Dev. Biol.* **139**, 61–88 (2020).
42. P. J. Scherz, B. D. Harfe, A. P. McMahon, C. J. Tabin, The limb bud SHH-FGF feedback loop is terminated by expansion of former ZPA cells. *Science* **305**, 396–399 (2004).
43. J. M. Verheyden, X. Sun, An FGF/Gremlin inhibitory feedback loop triggers termination of limb bud outgrowth. *Nature* **454**, 638–641 (2008).
44. S. Nissim, S. M. Hasso, J. F. Fallon, C. J. Tabin, Regulation of Gremlin expression in the posterior limb bud. *Dev. Biol.* **299**, 12–21 (2006).
45. P. Saiz-Lopez *et al*., An intrinsic timer specifies distal structures of the vertebrate limb. *Nat. Commun.* **6**, 8108 (2015).
46. D. Aguilar-Hidalgo *et al*., Critical point in self-organized tissue growth. *Phys. Rev. Lett.* **120**, 198102 (2018).
47. H. M. Choi *et al*., Third-generation in situ hybridization chain reaction: multiplexed, quantitative, sensitive, versatile, robust. *Development* **145**, dev165753 (2018).
48. R. Haase, D. Lee, D. D. Pop, L. Žigutytė, Napari-accelerated-pixel-and-object-classification: 0.14.1 (2023). Zenodo software repository. https://doi.org/10.5281/zenodo.10071078. Accessed 4 November 2023
49. C. L. Chiu *et al*., Napari: A Python multi-dimensional image viewer platform for the research community. *Microsc. Microanal.* **28**, 1576–1577 (2022).
50. N. Lyubaykina *et al*., Growth simulations and image analysis of Axolotl limb regeneration. Github repository. https://github.com/NataliaLyubaykina/axolotl_limb_regeneration_s. Deposited 18 August 2025.